Geophys. J. Int. (1994) **119,** 187–194

The pole–pole 3-D DC-resistivity inverse problem: a conjugate-gradient approach

R. G. Ellis and D. W. Oldenburg

Geophysical Inversion Facility, Department of Geophysics and Astronomy, University of British Columbia, Vancouver, Canada, V6T 1Z4

Accepted 1994 March 12. Received 1994 March 10; in original form 1993 July 24

SUMMARY

The pole–pole 3-D DC-resistivity inverse problem is solved by converting the inverse problem into an objective-function optimization problem, using the adjoint equation to compute the gradient of the objective function, and using a conjugate-gradient minimization. Two examples of the application of the resulting inversion algorithm are given. First, a large synthetic data set is inverted, and second, the inversion algorithm is used to invert E-SCAN field data of relevance to mineral exploration.

Key words: electrical resistivity, inverse problem.

1 INTRODUCTION

The DC-resistivity experiment is one of the oldest and simplest geophysical exploration techniques. From the pioneering work of the early 1900's (e.g. Slichter 1933) through to the present day there has been a steady evolution in DC resistivity in the areas of acquisition, inversion and interpretation. In the evolution of any process improvements in one area stimulate research efforts in other areas. In particular, in the DC-resistivity method there have been recent improvements in data acquisition that, combined with the development of powerful computer workstations, have stimulated the development of more sophisticated inversion algorithms. In this paper we present such an algorithm: a fully 3-D DC-resistivity inversion algorithm capable of producing minimum-structure conductivity models.

The first DC-resistivity experiments were restricted to sounding and profiling and intrinsically were restricted to 1- and 2-D environments. For example the familiar Schlumberger, Wenner, dipole–dipole, etc., arrays usually have colinear electrodes and do not provide sufficient information for a full 3-D interpretation of the area under investigation. This is not meant to imply that they cannot be used in 3-D environments, indeed, they frequently are used in such environments. However making a reliable 3-D interpretation based on a set of intrinsically 2-D profiles is not optimal. More satisfactory electrode geometries for 3-D environments can be constructed by allowing the potential electrodes to be moved off-line with respect to the current electrodes. One such generalization is the E-SCAN electrode configuration: in simple terms it is a pole–pole experiment in which a 2-D grid of electrodes is deployed and as each electrode in turn becomes the current electrode then the potential is measured at the remaining electrodes. It is not our purpose to discuss the details or merits of the E-SCAN acquisition technique and we refer the interested reader to the technical literature (Shore 1992). It is sufficient to note that E-SCAN data are truly 3-D and require a full 3-D inversion algorithm.

Any 3-D inversion algorithm designed for the solution of realistic geophysical inverse problems is going to burden today's computing facilities to their limit, primarily because the number of parameters in the model must be large enough to allow a minimum-structure model to simulate the real earth and because the number of data associated with a 3-D experiment is usually quite large. The inversion algorithm we present for the E-SCAN DC-resistivity experiment is no exception. However, the intrinsic simplicity of Poisson's equation makes this inverse problem tractable. Specifically after converting the inverse problem into an objective-function optimization problem, we use the adjoint equation to compute the gradient of the objective function, we map the gradient into a search direction in model space, and use a conjugate-gradients minimization. The large amount of data collected in an E-SCAN experiment prohibits the use of existing algorithms, e.g. methods that compute a sensitivity matrix (Park & Van 1991) would require the inversion of a matrix of $\sim 10^{13}$ elements for the problems considered in this paper. A full description of the inverse problem and our inversion algorithm is given in Section 2. In Section 4 the algorithm is applied to a large problem using synthetic data, and in Section 5 E-SCAN field data, collected over an area of epithermal mineralization, are inverted.

2 THE FORWARD PROBLEM

The DC-resistivity forward problem may be considered as a mapping from a space of conductivity models $\mathcal{M}$ to a space of potential data $\mathcal{D}$. The mapping from $\mathcal{M}$ to $\mathcal{D}$ is defined in terms of the self-adjoint linear-differential operator, L given

by

$$L[m]u = \nabla \cdot (m\nabla u) \qquad u \in \mathcal{D}, \quad m \in \mathcal{M}. \tag{1}$$

the space $\mathcal{M}$ will be taken to be the space of functions defined on a volume $\mathcal{V} \subset R^3$ satisfying the boundary conditions

$$\left.\frac{\partial m}{\partial n}\right|_{\partial\mathcal{V}} = 0$$
$$\left.\frac{\partial}{\partial n}(\nabla^2 m)\right|_{\partial\mathcal{V}} = 0. \tag{2}$$

The space $\mathcal{D}$ is taken to be the space of functions defined on $\mathcal{V}$ and satisfying prescribed boundary conditions on $\partial\mathcal{V}$. The boundary conditions associated with the DC-resistivity problem can be chosen in several different forms: various combinations of Dirichlet, Neumann, or mixed boundary conditions may be used. Since we must ultimately revert to numerical techniques we choose the mixed boundary conditions (see Fig. 1) which are well suited to numerical simulation (Dey & Morrison 1979),

$$\left.\frac{\partial u}{\partial n}\right|_{\partial\mathcal{V}} = 0 \quad \text{on} \quad z = 0$$
$$\left.\frac{\partial u}{\partial n} + \frac{\cos\varphi}{r}u\right|_{\partial\mathcal{V}} = 0 \quad \text{on} \quad z \neq 0. \tag{3}$$

With the same boundary conditions for the adjoint operator $L^* = L$ it can be shown that L is symmetric with respect to functions $u, v \in \mathcal{D}$, i.e.

$$\int_{\mathcal{V}} v(x)Lu(x)\,dx^3 = \int_{\mathcal{V}} u(x)Lv(x)\,dx^3. \tag{4}$$

The DC-resistivity forward problem, with current sources, requires the solution of the inhomogeneous equation,

$$L[m]u = -\phi(\mathbf{x}) \qquad u \in \mathcal{D}, \qquad m \in \mathcal{M}, \quad x \in R^3 \tag{5}$$

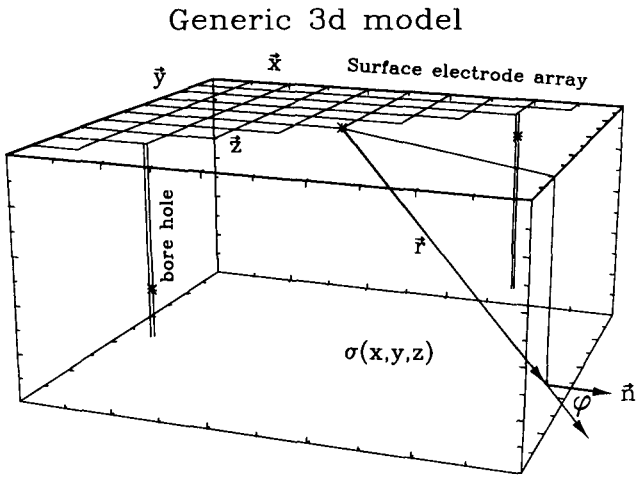

Figure 1. A representation of the volume $\mathcal{V}$ defining the domain for the DC-resistivity forward modelling. Within this domain the conductivity is denoted by $\sigma(x, y, z)$. From the centre of the surface a vector $\mathbf{r}$ can be drawn to any point on the boundary $\partial\mathcal{V}$, $\hat{\mathbf{n}}$ is the normal to the surface $\partial\mathcal{V}$ and ϕ is the angle between $\hat{\mathbf{n}}$ and $\mathbf{r}$. Current and potential electrodes may be placed on the surface $z = 0$, usually in a rectangular grid, or at boreholes in $\mathcal{V}$.

where ϕ is a generalized function usually representing point current sources by Dirac δ functions. Consequently, we introduce the Green's function $G[m](\mathbf{x}_1; \mathbf{x}_2)$ such that,

$$L[m]G[m](\mathbf{x}; \mathbf{x}_0) = -\delta(\mathbf{x} - \mathbf{x}_0). \tag{6}$$

The Green's function is required to satisfy the boundary conditions eq. (3).

Using the Green's function the solution of eq. (5) is given by,

$$u(\mathbf{x}_1) = \int_{\mathcal{V}} G[m](\mathbf{x}_1; \mathbf{x}_2)\phi(\mathbf{x}_2)\,dx_2^3. \tag{7}$$

We note that a self-adjoint differential operator has a symmetric Green's function, i.e.

$$L[m] = L^*[m] \Rightarrow G[m](\mathbf{x}_1; \mathbf{x}_2) = G[m](\mathbf{x}_2; \mathbf{x}_1). \tag{8}$$

3 THE INVERSE PROBLEM

The DC-resistivity inverse problem may be considered as a mapping from the space of the potential data $\mathcal{D}$ to the space of conductivity models $\mathcal{M}$. For example, the inverse problem may be stated as, given $u \in \mathcal{D}$ find $m \in \mathcal{M}$ such that eqs (5, 3) are satisfied. More realistically, in a DC-resistivity experiment a set of N potential measurements and associated errors are acquired. Let us denote the measurement locations by $\mathbf{x}_i^{\text{obs}}$, $i = 1, \ldots, N$ and the associated potentials and errors by d_i^{obs}, $i = 1, \ldots, N$ and δd_i^{obs}, $i = 1, \ldots, N$. The practical inverse problem then becomes, given N potential measurements d_i^{obs} with errors δd_i^{obs} find an $m \in \mathcal{M}$ such that eqs (5, 3) are satisfied. This inverse problem is clearly ill-posed (Tikhonov & Arsenin 1977).

One approach to ill-posed inverse problems is to recast the original problem in the form of a regularized optimization problem. For example the preceding inverse problem may be written in terms of an objective function $S[m]$ with two contributions; a data-misfit measure and a model character measure i.e.

$$S[m] = \sum_{i=1}^{N}\left(\frac{d_i^{\text{obs}} - d_i^{\text{cal}}[m]}{\delta d_i^{\text{obs}}}\right)^2 + \mu\int_{\mathcal{V}}(W[m(x)])^2\,dx^3 \tag{9}$$

where

$$d_i^{\text{cal}}[m] = \int_{\mathcal{V}} \delta(\mathbf{x}_i^{\text{obs}} - \mathbf{x})u[m](\mathbf{x})\,dx^3 \qquad u \in \mathcal{D} \quad m \in \mathcal{M}. \tag{10}$$

μ is a regularization parameter, and W is any operator operating on m. The first term in eq. (9) is a measure of the misfit between the predicted data and the observed data while the second term is a measure of model character. For example if W was the Laplacian operator the second term in eq. (9) would be a measure of the 'smoothness' of the model. Note that the regularization parameter μ functions as a trade-off parameter between the two terms in $S[m]$.

The solution m^* to this practical inverse problem is simply given by,

Find m^* such that $S[m^*]$ is a minimum.

In this form the problem is well posed and can be solved by the techniques of conventional optimization theory.

A number of particularly efficient optimization algorithms

for large-scale problems are based on finding a search direction in the space of models and performing a univariate minimization of S along that search direction. When a minimum is found a new search direction is chosen. Frequently the gradient of the objective function is used in the generation of a search direction: for example, in the steepest-descent algorithm only the gradient of the objective function at the current model estimate is used in forming the search direction; alternatively, in the conjugate-gradient algorithm the search direction is chosen to be the component of the gradient of the objective function at the current model estimate conjugate to the preceding search directions. Consequently an efficient method of computing the gradient of the objective function is required.

The derivation of the gradient of $S[m]$ is particularly straightforward in the case where L is self-adjoint. To simplify the derivation we split the objective function $S[m]$ into two parts,

$$S[m] = S_D[m] + \mu S_M[m]$$
$$S_D[m] = \sum_{i=1}^{N} \left(\frac{d_i^{\text{obs}} - d_i^{\text{cal}}[m]}{\delta d_i^{\text{obs}}} \right)^2 \tag{11}$$
$$S_M[m] = \int_{\mathcal{V}} (Wm(x))^2 \, dx.$$

Let us first consider the variation in the data-misfit contribution $S_D[m]$ under perturbations of the model and define $\delta S_D[m]$ by,

$$S_D[m + \delta m] = S_D[m] + \delta S_D[m]. \tag{12}$$

Substituting for $S_D[m]$ yields

$$S_D[m + \delta m] = \sum_{i=1}^{N} \left(\frac{d_i^{\text{obs}} - d_i^{\text{cal}}[m + \delta m]}{\delta d_i^{\text{obs}}} \right)^2. \tag{13}$$

Next substituting for d_i^{cal} using the projection eq. (10) and the Green's function eq. (7) yields

$$S_D[m + \delta m] = \sum_{i=1}^{N} \frac{1}{(\delta d_i^{\text{obs}})^2} \times \left(d_i^{\text{obs}} - \int_{\mathcal{V}} G[m + \delta m](\mathbf{x}_i; \mathbf{x}) \phi(\mathbf{x}) \, dx^3 \right)^2. \tag{14}$$

Writing

$$G[m + \delta m] = G[m] + \delta G[m] \tag{15}$$

and substituting yields,

$$\delta S_D[m] = 2 \sum_{i=1}^{N} \frac{d_i^{\text{obs}} - d_i^{\text{cal}}}{(\delta d_i^{\text{obs}})^2} \int_{\mathcal{V}} \delta G[m](\mathbf{x}_i; \mathbf{x}) \phi(\mathbf{x}) \, dx^3. \tag{16}$$

Using the relationship between the Green's function and the differential operator, eq. (6) it can be shown to first order that,

$$\delta G[m](\mathbf{x}_1; \mathbf{x}_2) = \int G[m](\mathbf{x}_1; \mathbf{x}_3) \delta L[m] G[m](\mathbf{x}_3; \mathbf{x}_2) \, dx_3^3 \tag{17}$$

where

$$L[m + \delta m] = L[m] + \delta L[m]. \tag{18}$$

Substituting eq. (17) into eq. (16) and manipulating yields

$$\delta S_D[m] = 2 \sum_{i=1}^{N} \frac{d_i^{\text{obs}} - d_i^{\text{cal}}}{(\delta d_i^{\text{obs}})^2} \times \int_{\mathcal{V}} G[m](\mathbf{x}_i; \mathbf{x}) \delta L[m] d^{\text{cal}}(\mathbf{x}) \, dx^3 \tag{19}$$

using the symmetry of the Green's function this can be rewritten,

$$\delta S_D[m] = 2 \int_{\mathcal{V}} g[m](\mathbf{x}) \delta L[m] d^{\text{cal}}(\mathbf{x}) \, dx^3 \tag{20}$$

where

$$g[m](\mathbf{x}) = \sum_{i=1}^{N} G[m](\mathbf{x}; \mathbf{x}_i) \frac{d_i^{\text{obs}} - d_i^{\text{cal}}}{(\delta d_i^{\text{obs}})^2}. \tag{21}$$

For L defined in eq. (1) we have

$$\delta S_D[m] = 2 \int_{\mathcal{V}} g[m](\mathbf{x}) \nabla \cdot (\delta m(\mathbf{x}) \nabla d^{\text{cal}}(\mathbf{x})) \, dx^3. \tag{22}$$

This expression relates a change in the model δm to a change in the objective function δS_D.

At this stage it is particularly convenient to further restrict the space of models to the Hilbert space described by the algebraic span of a set of orthogonal basis functions $\psi_i(\mathbf{x})$, $i = 1, \ldots, M$ defined on $\mathcal{V}$, i.e.

$$m(\mathbf{x}) = \sum_{i=1}^{M} m_i \psi_i(\mathbf{x}) \tag{23}$$

with the model perturbations being,

$$\delta m(\mathbf{x}) = \sum_{i=1}^{M} \delta m_i \psi_i(\mathbf{x}). \tag{24}$$

With this form of model perturbation we have

$$\delta S_D[m] = 2 \sum_{i=1}^{M} \delta m_i \int_{\mathcal{V}} g[m](\mathbf{x}) \nabla \cdot (\psi_i(\mathbf{x}) \nabla d^{\text{cal}}(\mathbf{x})) \, dx^3, \tag{25}$$

and it follows that the gradient of the objective function S_D with respect to the parametrized model space is

$$\frac{\partial S_D[m]}{\partial m_i} = 2 \int_{\mathcal{V}} g[m](\mathbf{x}) \nabla \cdot (\psi_i(\mathbf{x}) \nabla d^{\text{cal}}(\mathbf{x})) \, dx^3. \tag{26}$$

Now let us consider the variation in the model character contribution S_M to the objective function, eq. (11) under perturbations of the model. We define $\delta S_M[m]$ by,

$$S_M[m + \delta m] = \int (W(m + \delta m))^2 \, dx^3 = S_M[m] + \delta S_M[m]. \tag{27}$$

Substituting for $S_M[m]$ we consider the special case where W is given by the Sobolov–Laplacian (e.g. Naylor & Sell 1982)

operator

$$S_m[m] = \int (Wm(\mathbf{x}))^2\, dx^3$$

$$= \int (1-\epsilon)^2 |\nabla\nabla^2 m|^2 + 2\epsilon(1-\epsilon)|\nabla m|^2 + \epsilon^2 |m|^2\, dx^3 \quad 0 < \epsilon \leq 1$$

$$= \int ((1-\epsilon)\nabla^2 m - \epsilon m)^2\, dx^3. \tag{28}$$

This apparently cumbersome operator is in fact particularly easy to implement numerically and has the mathematically necessary property, ensured by the non-zero parameter ϵ, that it defines a proper norm (the Laplacian is a semi-norm). In more physical terms, the parameter ϵ controls the type of model that will be produced in the inversion: if ϵ is small the final model will be a 'smooth' model; if $\epsilon \sim 1$ the final model will be a 'small' model. The numerical implementation is as follows. A functional perturbation of the conductivity yields

$$S_M[m+\delta m] = \int_V ((1-\epsilon)\nabla^2(m+\delta m) - \epsilon(m+\delta m))^2\, dx^3$$

$$= S_M[m] + 2\int_V \delta m((1-\epsilon)\nabla^2 - \epsilon)((1-\epsilon)\nabla^2 - \epsilon)m\, dx^3, \tag{29}$$

where we have used the boundary conditions eq. (2) and made use of Green's theorem. This expression relates a change in the model δm to a change in the objective function contribution δS_M. After parametrizing the model via eq. (23) we have

$$\frac{\partial S_M[\sigma]}{\partial m_i} = 2\int_V \psi_i(\mathbf{x})((1-\epsilon)\nabla^2 - \epsilon)((1-\epsilon)\nabla^2 - \epsilon)m(\mathbf{x})\, dx^3. \tag{30}$$

The gradient of the total objective function $S[m]$, which we denote by $\hat{\gamma}$, with respect to changes in the model parameters is given by the sum of eq. (26) and eq. (30).

Before the gradient can be used to define a steepest-descent direction in the model space $\mathcal{M}$ it is necessary to define a norm on $\mathcal{M}$ (Gill, Murray & Wright 1981). The steepest-descent direction depends on the choice of norm and it is natural to choose the W-weighted l_2-norm associated with the model measure in the objective function. The steepest-ascent direction, γ, and the gradient direction are related by

$$W'[W[\gamma]] = \hat{\gamma}. \tag{31}$$

Assuming that it is possible to define, or at least to approximate numerically, the inverse operator $(W'W)^{-1}$ by,

$$\gamma = (W'W)^{-1}\hat{\gamma} \tag{32}$$

then the steepest-descent direction under the W-weighted l_2-norm can be computed and used to construct a search direction $p(x)$ along which a univariate minimization can be performed.

In our applications the search direction $p(x)$ is formed as given in the method of conjugate gradients for non-quadratic functionals (Hestenes 1980). We use the following algorithm (Polyak & Ribiere 1969),

Choose $m^{(1)}$ and set $r^{(1)} = -\gamma(m^{(1)})$, $p^{(1)} = r^{(1)}$.

Choose $\alpha = \alpha^k$ to minimize $S(\alpha) = S(m^{(k)} + \alpha p^{(k)})$

$$m^{(k+1)} = m^{(k)} + \alpha^k p^{(k)} \qquad r^{(k+1)} = -\gamma(m^{(k+1)}).$$

When $\frac{k}{n}$ is an integer set $p^{(k+1)} = r^{(k+1)}$ otherwise set (33)

$$p^{(k+1)} = r^{(k+1)} + b^k p^{(k)}, \qquad b^k = \frac{|r^{(k+1)}|^2 - r^{(k)} \cdot r^{(k+1)}}{|r^{(k)}|^2}$$

Terminate at the jth step if $|r^{(j+1)}|$ is sufficiently small.

In theory, the algorithm is reset every n iterations, where n is the number of parameters in the model. However, in practice the algorithm usually converges before the nth iteration.

4 NUMERICAL CONSIDERATIONS

A minimum-structure inversion algorithm should produce inversion results that are not dependent on the model parametrization. Consequently such algorithms must be based on finely discretized models which, in three dimensions, leads to models with a large number of parameters. This translates into memory and disk storage, and CPU (central processing unit) implications for the numerical implementation.

The more important constraint from a numerical viewpoint is the CPU time required for the inversion. By far the most CPU-intensive part of a conjugate-gradient algorithm is forward modelling that is necessary to compute the data for a given model, the value of the objective function, and as implied in eq. (26), the gradient of the objective function. Further, a univariate minimization must be performed at each iteration of the conjugate gradient algorithm. These considerations indicate the need for an optimum univariate minimization algorithm and an optimum forward-modelling algorithm.

A number of different univariate-minimization algorithms were tested with the optimum algorithm based on cubic interpolation (Acton 1970) and requiring on average four implementations of the forward-modelling program per conjugate-gradient iterations.

The forward modelling was performed with a finite-difference approximation to the physical equations. The numerical implementation used the Dey & Morrison (1979) capacitance matrix and an iterative sparse matrix solver developed at the University of Waterloo (D'Azevedo, Knightley, & Forsyth 1991). An iterative solver is well suited to the inverse problem because a similar forward problem has to be solved many times. Using an iterative method the solution from a past forward modelling can be used as the starting point for the next forward modelling. This simple re-use of solutions can substantially reduce CPU time.

The appropriate choice of data and model are important considerations in any inverse problem. In this work the data

were taken to be $\ln V$ and the model to be $\ln \sigma$. With these choices the large dynamic range in both V and σ are reduced, giving a more stable and more convergent algorithm.

5 A SIMPLE FIVE PRISM MODEL

In this section we apply the conjugate-gradient algorithm described above to invert synthetic data from a test model consisting of five prisms as shown in Fig. 2. This model was originally proposed by Li & Oldenburg (1994) as a test model for 3-D DC-resistivity inversion. It consists of three surface prisms (S1, S2, S3) of resistivities 100, 200 and 2000 Ωm and two buried prisms (B1, B2) of resistivities of 2000 and 100 Ωm all in a 1000 Ωm background half-space. The surface prisms are designed to simulate near surface-conductivity variations and the buried prisms are the survey targets. The model was discretized into $n_x \times n_y \times n_z = 17{,}496$ cells, where $(n_x, n_y, n_z) = (27, 27, 24)$.

We consider the inversion of a data set produced from this model. The starting model was chosen to be a uniform half-space of 1000 Ωm. The data consist of high-density surface data collected on a uniform square array of 21×21 electrodes placed on a 50 m grid. The electrode array was centred on the model space shown in Figs 2 and 3. Each electrode was taken as a current electrode and potentials were recorded from all electrodes in the electrode array within a radius of 500 m. This yields a total 87,688 potential data. Unbiased Gaussian noise of 1 per cent was added to the potentials before inversion. Data collected from a single current electrode, before noise was added, is shown in Fig. 3.

The result of applying the conjugate-gradient algorithm described above to the synthetic data with noise added produced the following inversion results. We chose to fit the potential data to an rms misfit of 1.0 per cent. The results of the inversion are shown in Fig. 4 where we display three slices through the true model and the inversion result. Fig. 4 consists of six panels; the three on the right correspond to slices through the true model, the three on the left correspond to the inversion result. The upper images are vertical slices at $X = 475$ m, the middle images are near surface horizontal slices with $Z = 20$ m, and the lower images are deeper horizontal slices through the targets at $Z = 500$ m. The inversion took 39 iterations, and in total, including objective function gradient modelling, 97 applications of the forward-modelling algorithm. Fig. 5 shows the total objective function as a function of iteration and illustrates a practical aspect of the inversion algorithm: the choice of trade-off parameter μ. Since the appropriate value of μ, which corresponds to a particular data misfit and model roughness, is not known at the beginning of the inversion, some estimate must be made. In practice, an initial value μ_1 is chosen and several iterations performed. If the convergence plot, Fig. 5, begins to plateau at an excessive rms misfit, then a smaller value, μ_2, of the trade-off parameter is chosen. This trial and error method of finding a desired trade-off parameter quickly results in suitable data misfit. In this example three different values of μ were used to reach a rms data misfit of 1.0 per cent rms.

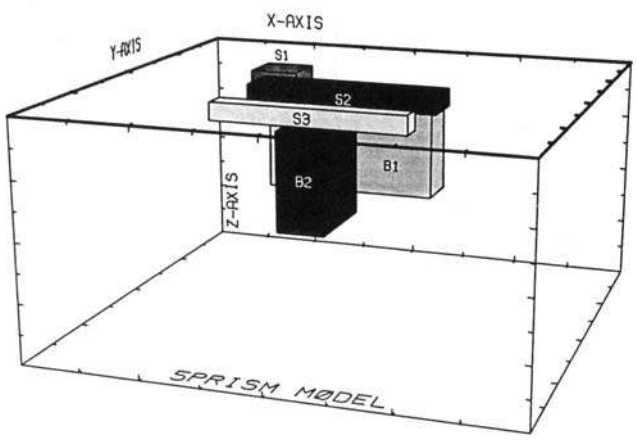

Figure 2. A perspective view of the five-prism model. The model consists of three surface prisms (S1, S2, S3) with resistivities of 100, 200, and 2000 Ωm and two buried prisms (B1, B2) of resistivities of 2000 and 100 Ωm. The surface prisms extend from surface to a depth of 40 m, the buried prism B1 extends from depth 50–250 m and the buried prism B2 extends from 95–275 m.

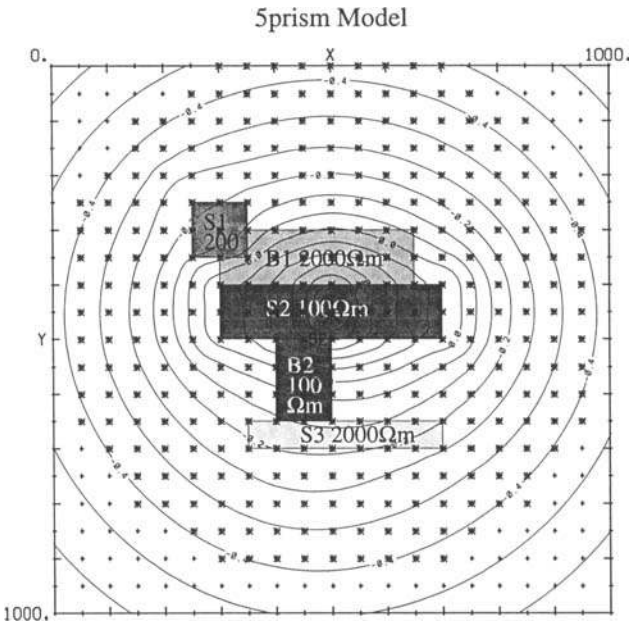

Figure 3. A plan view of the five-prism model (Fig. 2) showing the outline of the anomalous prisms, the current and potential electrode locations (+), and the electrodes at which the data is collected (*) for a single current source. Also shown are contours of constant $\log V$.

Several features of the inversion result are worth special attention. First, the model is generally well resolved. The large conductive buried target prism is clearly visible in the vertical sections Fig. 4 (upper panels) and the deep horizontal sections Fig. 4 (lower panels). Less obvious but still clearly visible, in the same panels, is the buried resistive target prism. The two conductive surface prisms are very clearly seen in Fig. 4 (middle panels), however, the resistive surface prism is partially obscured by a general high-resistivity zone over the top of the conductive prism. This lack of resolution is due primarily to the implementation of a globally smoothest model, and the usual observation that resistive bodies are harder to detect than conductive bodies by electrical methods.

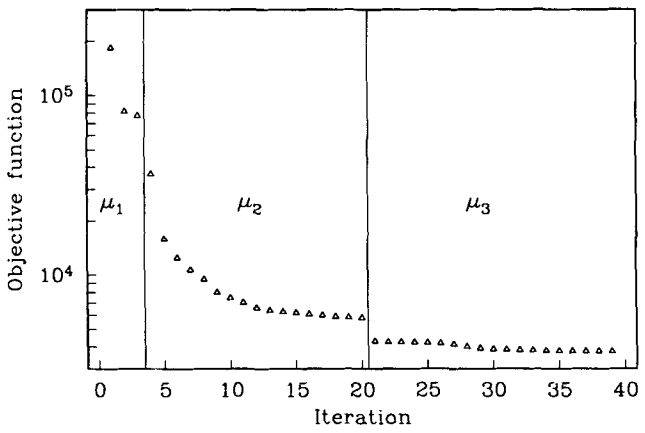

Figure 5. The convergence plot for the inversion resulting in the model shown in Fig. 4. The total objective function, S, is shown (△) as a function of iteration. The plot is divided into three regions each corresponding to a different value of trade-off parameter μ. The data misfit converges to an rms = 1.0 per cent.

6 INVERSION OF FIELD DATA

While synthetic data are necessary for testing and measuring the performance of inversion algorithms they are frequently much better behaved than geophysical field measurements. We have tested the conjugate-gradient inversion algorithm described above on a field data set. The data were collected with the E-SCAN acquisition system yielding high-density coverage with surface electrodes over a region associated with epithermal mineralization, but covered with eluvium.

A typical model for epithermal mineralization is one in which a high-level hydrothermal fluid ascending toward the surface, undergoes cooling and chemical changes with resulting mineralization that takes place in a near-surface to surface hot-spring environment. Usually zones of mineralization form along a dominant subvertical fracture system. These extend from a depth of about 500 m up to the surface where they split into a number of subsidiary structures. This gives rise to a mushroom-shaped propylitic envelope that in turn gives the deposit its characteristic signature: a resistive mushroom-shaped anomaly.

In an attempt to identify epithermal mineralization beneath the eluvium, data were acquired over a flat-square region, approximately 2 km by 2 km, known as Site A. The electrodes were spaced in a square grid with spacing 91.4 m. The E-SCAN data were acquired in a manner such that, after some use of reciprocity, a total of 10,000 measurements of the potential were collected from a total of 121 current electrodes. The potential measurement sites relative to a typical current electrode are shown in Fig. 6. The real acquisition electrode layout is related to the details of the E-SCAN method which is not the focus of our work, and hence will not be discussed in this paper. For the purposes of inversion it is sufficient to know that the effective experiment consisted of current electrodes located at every second electrode site i.e. on a square grid with spacing 182.88 m, and that potentials electrodes were located at sites on the 91.4 m grid in the vicinity of the activated current electrode, Fig. 6.

The first procedure in analysing the field data was to make some assessment of data quality, i.e. estimate the total error

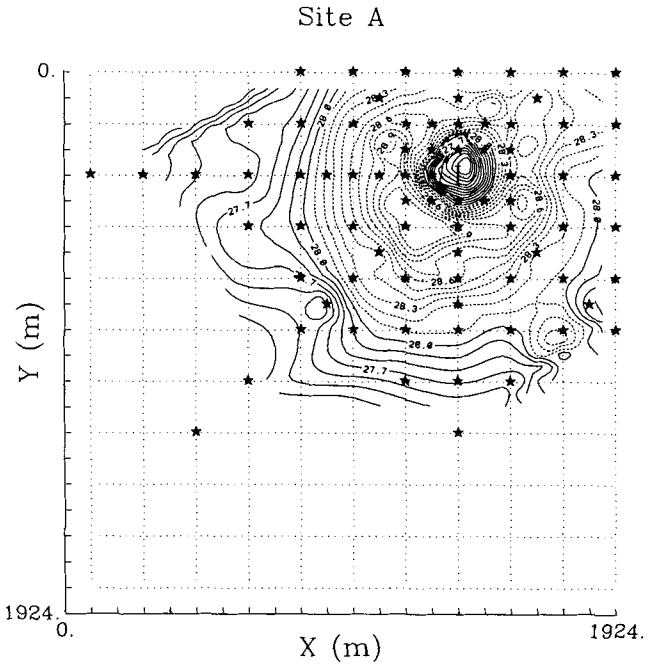

Figure 6. Plan view of Site A, a topographically flat region 1924 m × 1924 m in extent. Current electrodes were placed on a square grid with grid spacing 182.88 m, shown as dashed lines. Potential electrodes were placed surrounding the current electrode in a configuration typified by the ★ symbol surrounding the current located at I. The potential electrodes all lie on a square grid with grid spacing 91.44 m. Contours are of $-10*\log_{10}(r*V)$ where V is the measure potential in Volts and r is the distance between the potential electrode and the current electrode.

associated with each measurement. A partial estimate of the error can be made by statistical analysis of the voltage stack, however errors from other sources cannot be estimated during acquisition. Consequently, in order to get a working estimate of the errors, we applied a generalized-cross-validation (GCV) 2-D thin-plate smoothing spline (Craven & Wahba 1979) to the raw data $(r*V)$ to generate smoothed data. A comparison between typical raw data and smoothed data can be made by comparing Figs 6 and 7. We then assumed that the smoothed data approximately represented noise-free data and that the difference between the smoothed data and the raw data could be taken as a relative measure of the standard deviation of the error associated with each raw datum. With this assumption we have an estimate for δd_i^{obs} in eq. (11). This method for estimating the data error is rather *ad hoc*, however, we have found that the final model produced by the inversion algorithm is rather insensitive to the assignment of errors due to redundancy in the data.

Inverting the field data we produced a model that fit the data to ~6 per cent in 30 iterations. The starting model was a uniform half-space of resistivity 18 Ωm. The character of the final model can be seen in Fig. 8 (upper panel) which show a 10 Ωm and a 50 Ωm isosurface (lower panel). In Fig. 8 (upper panel) all resistivities less than 10 Ωm are contained within the isosurface, and in Fig. 8 (lower panel) all resistivities greater than 50 Ωm are contained in the isosurface. Fig. 8 (lower panel) shows several resistive zones

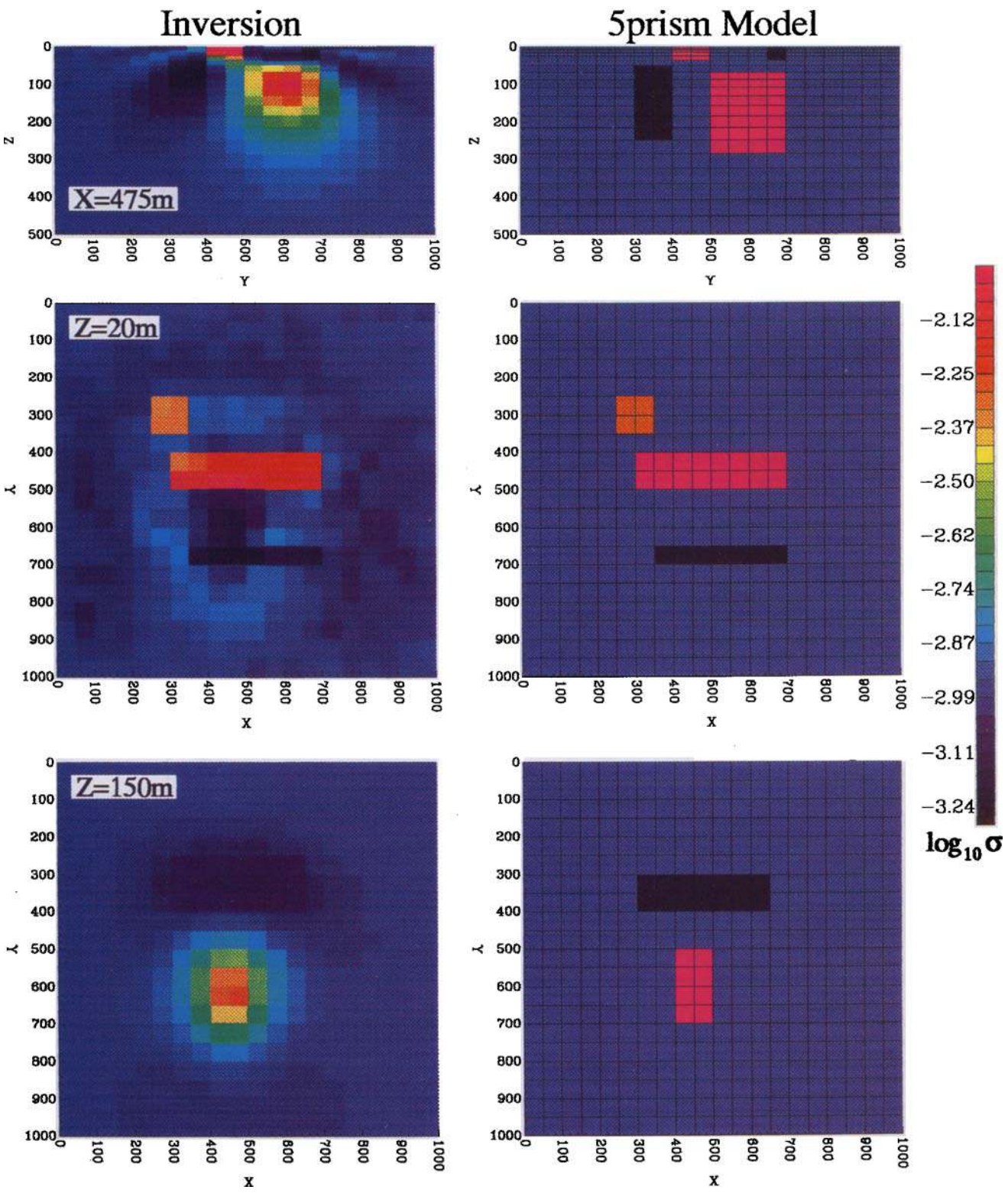

Figure 4. Three slices through the five-prism conductivity model (right) and the corresponding slices for the inversion result (left). The upper panel is a vertical section through the model at $x = 475$ m, the middle panel is a horizontal section at $z = 20$ m and the lower panel is a horizontal section at $z = 150$ m. The colour bar shows $\log_{10} \sigma$ and applies to all panels, the vertical and horizontal axes are in metres.

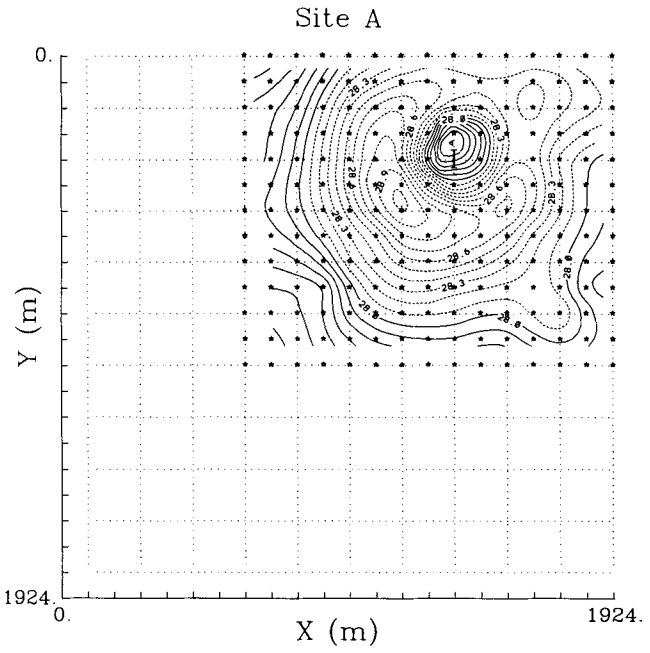

Figure 7. The layout and contour plot analogous to Fig. 6, for the GCV thin-plate smoothing splined data.

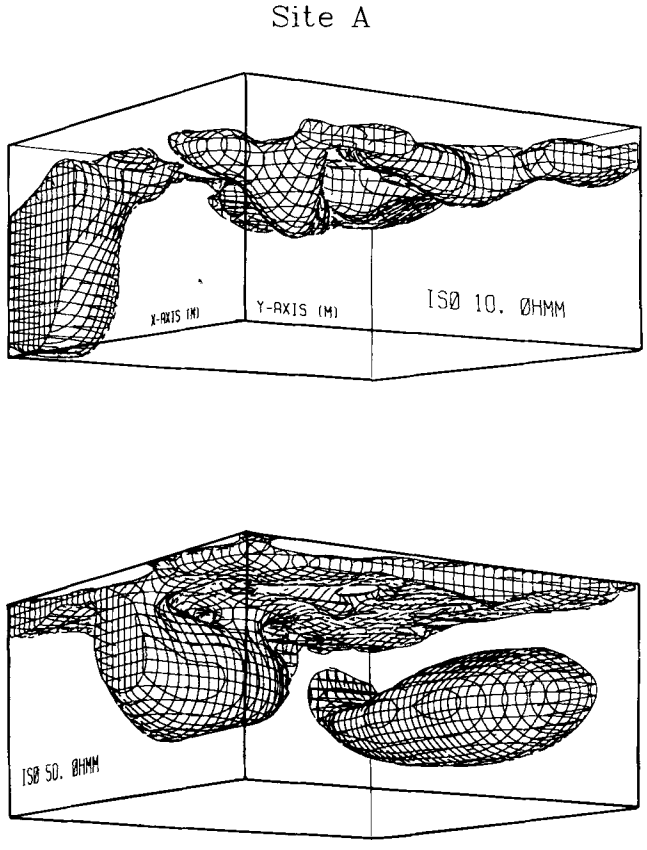

Figure 8. Isoresistivity contours showing a 10 Ωm and 50 Ωm isosurface. In the upper image all resistivities less than 10 Ωm are contained within the isosurface, and in lower image all resistivities greater than 50 Ωm are contained in the isosurface.

extending from depth to near surface, which have the potential of being epithermal deposits.

7 CONCLUSION

Recent advances in DC-resistivity data acquisition, for example the E-SCAN system, and the development of high-power workstations have made the inversion of 3-D DC-resistivity data necessary and feasible. The need for such an inversion inspired the development of the conjugate-gradient DC-resistivity inversion described and tested in this paper.

3-D inverse problems usually involve large numbers of model parameters and large amounts of data. Hence, inverse methods that depend on Frechet derivative matrices are of limited utility. Instead the inverse problem may be converted to an optimization problem that can then be solved via the method of conjugate gradients, provided an efficient method of computing the gradient of the objective function can be found. We have shown how that gradient can be computed by using the Green's function method with the same cost as single forward modelling.

The conjugate-gradient inversion has been tested on synthetic data and on field data and has been found to be reliable and efficient. The models that are produced not only fit the data but also have minimum structure. This is an important consideration since the 3-D DC-resistivity inverse problem is non-unique and any inversion algorithm will produce only one of many possible models that fit the data to a given misfit level. However, if the model has a minimum model norm, then we may expect that anomalies in the final model are required by the data. This is a significant point for mineral exploration.

ACKNOWLEDGMENTS

The authors would like to thank Y. Li for useful discussions and to acknowledge FMC Gold Company and Premier Geophysics for financial assistance and for providing the field data. This work was supported by NSERC/Industry CRD grant 5-80141.

REFERENCES

Acton, F.S., 1970. *Numerical methods that Work*, Harper & Row, New York.

Craven, P. & Wahba, G., 1979. Smoothing noisy data with spline functions: estimating the correct degree of smoothing by the method of generalized cross-validation, *Numer. Math.*, **31**, 377–403.

D'Azevedo, E.F., Knightly, J.R. & Forsyth, P.A., 1991. *MATI Iterative Sparse Matrix Solver: User's Guide*, Department of Computer Science, University of Waterloo, Ontario.

Dey, A. & Morrison, H.F., 1979. Resistivity modelling for arbitrary shaped three-dimensional structures, *Geophysics*, **44**, 753–780.

Gill, P.E., Murray, W. & Wright, M.H., 1981. *Practical Optimization*, Academic Press, New York.

Hestenes, M.R., 1980. *Conjugate Directions Methods in Optimization*, Springer-Verlag, New York.

Li, Y. & Oldenburg, D.W., 1994. Inversion of 3-D DC resistivity data using an approximate inverse mapping, *Geophys. J. Int.*, **116**, 527–537.

Naylor, A.W. & Sell, G.R., 1982. *Linear Operator Theory in Engineering and Science,* Springer-Verlag, New York.

Park, S.K. & Van, G.P., 1991. Inversion of pole-pole data for 3D resistivity structure beneath arrays of electrodes, *Geophysics,* **56,** 951–960.

Polyak, E. & Ribiere, G., 1969. Note sur la convergences des methodes conjuges, *Rev. Fr. Inr. Rech. Oper.,* **16,** 35–43.

Shore, G., 1992. *E-SCAN Resource Mapping: Multidirectional Electrical Surveys,* Premier Geophysics Inc., Richmond, B.C., Canada.

Slichter, L.B., 1933. The interpretation of the resistivity prospecting method for horizontal structures, *Physics,* **4,** 307–322.

Tikhonov, A.N. & Arsenin, V.Y., 1977. *Solutions of Ill-posed Problems,* ed. Fritz, J., John Wiley & Sons, New York.